

# Segmentation of Hemodynamics from Dynamic-Susceptibility-Contrast Magnetic Resonance Brain Images Using Sequential Independent Component Analysis

Yu-Te Wu<sup>1,4</sup>, Hui-Yun Chen<sup>1,4</sup>, Chih-I Hung<sup>1,4</sup>, Yi-Hsuan Kao<sup>1</sup>,  
Wan-Yuo Guo<sup>3,5</sup>, Tzu-Chen Yeh<sup>3,4</sup>, Jen-Chuen Hsieh<sup>2,3,4</sup>

<sup>1</sup>Institute of Radiological Sciences, <sup>2</sup>Institute of Neuroscience, <sup>3</sup>Faculty of Medicine, School of Medicine, National Yang-Ming University No.155, Sec. 2, Linong St., Beitou District, 112, Taipei, Taiwan,

<sup>4</sup>Integrated Brain Research Laboratory, Dept. of Medical Research and Education, <sup>5</sup>Department of Radiology, Taipei Veterans General Hospital, No.201, Sec. 2, Shihpai Rd., Beitou District 112, Taipei, Taiwan

e-mail : [ytwu@ym.edu.tw](mailto:ytwu@ym.edu.tw); [airrb@pchome.com.tw](mailto:airrb@pchome.com.tw); [runtothewater@pie.com.tw](mailto:runtothewater@pie.com.tw); [yhkao@ym.edu.tw](mailto:yhkao@ym.edu.tw), [wgyuo@vghtpe.gov.tw](mailto:wgyuo@vghtpe.gov.tw), [cych@vghtpe.gov.tw](mailto:cych@vghtpe.gov.tw), [jchsieh@vghtpe.gov.tw](mailto:jchsieh@vghtpe.gov.tw)

## ABSTRACT

Dynamic-susceptibility-contrast magnetic resonance imaging, a popular perfusion imaging technique, records signal changes on images caused by the passage of contrast-agent particles in the human brain after a bolus injection of contrast agent. The temporal signal changes on different brain tissues characterize distinct blood supply patterns which are critical for the profound analysis of cerebral hemodynamics. Under the assumption of the spatial independence among these patterns, independent component analysis (ICA) was applied to segment different tissues, i.e., artery, gray matter, white matter, vein and sinus and choroids plexus, so that the spatio-temporal hemodynamics of these tissues were decomposed and analyzed. An arterial input function was modeled using the concentration-time curve of the arterial area for the deconvolution calculation of relative cerebral blood flow. The cerebral hemodynamic parameters, such as relative cerebral blood volume (rCBV), relative cerebral blood flow (rCBF), and relative mean transit time (rMTT), were computed and their averaged ratios between gray matter and white matter were in good agreement with those in the literature.

## Keywords

Cerebral blood Hemodynamics, magnetic resonance imaging (MRI), independent component analysis (ICA), image segmentation

## 1. INTRODUCTION

Extraction of differently regional blood flow in brain is vital for the analysis of brain perfusion and

assessment of cerebral-vascular diseases. By using the dynamic-susceptibility-contrast (DSC) MR imaging tool, signal changes embodying different blood supply patterns can be recorded after injecting a bolus of contrast agent intravenously [Aro95a, Guc96a, Ost96a, Rem94a, Ros90a, Sor97a]. With the bolus profile of arterial compartment being identified, cerebral hemodynamic parameters, namely cerebral blood volume (CBV), cerebral blood flow (CBF), and mean transit time (MTT), can be computed based on indicator dilution theory [Zie65a]. It has been demonstrated that the hemodynamic parameter maps have important clinical applications, including the

Permission to make digital or hard copies of all or part of this work for personal or classroom use is granted without fee provided that copies are not made or distributed for profit or commercial advantage and that copies bear this notice and the full citation on the first page. To copy otherwise, or republish, to post on servers or to redistribute to lists, requires prior specific permission and/or a fee.

WSCG'2004, February 2-6, 2004, Plzen, Czech Republic.  
Copyright UNION Agency – Science Press

assessment of brain tumors [Aro95a; Ost96a; Sor97a], brain ischemia [Ros90a; Ost96a; Sor97a], occlusive cerebral-vascular disease [Guc96a], and radiation necrosis [Aro95a; Sor97a].

It is desirable to classify bolus transit profiles into different clusters so as to group together spatially distributed tissues with similar temporal signal-time curves. The segmentation of spatio-temporal hemodynamics enables us to 1) extract the arterial area and model a brain-feeding arterial input function in plane, rather than use the carotid, vertebral or middle cerebral artery at a remote slice location [Rem94a, Guc96a, Ost96a], for accurate estimation of rCBV and rCBF; 2) segment regions enduring perfusion deficiency for facilitating the diagnosis and staging of brain diseases. To classify signal-time curves of perfusion images, a commonly used method is to manually select single or multiple pixels for the tissue of interest and employ their temporal profiles to form a reference function in producing a similarity map. Pixels with large intensities on such a map have highly temporal correlations with the reference function and can be classified into the same group via thresholding. This method has been applied to segment astrocytoma and cysts [Rog94a], and to dissect gray and white matter from perfusion images [Wia01a]. While this method is advantageous on easy implementation, it is, however, limited to extraction of single tissue pattern per similarity map. When different tissue patterns are to be segmented out, multiple similarity maps are required which mandate cumbersome selections of reference pixels and are prone to operator influence.

Independent component analysis (ICA), a data-driven method for multivariate data analysis, is a promising tool that attempts to separate mixed signals into independent source components [Hyv97a, Hyv01a]. Such a 'blind source separation' process has successful applications on magnetoencephalographic data to reveal temporally independent neuronal activities [Lee03a], on MR perfusion images to identify and remove the confounding signals of large blood vessels from hemodynamic parameter maps [Car02a], on  $T_2$  and diffusion-weighted images to separate a portion of noise content within the diffusion tensor imaging datasets [Arf02a], and on dynamic  $H_2^{15}O$  PET images to separate the ventricles and myocardium [Lee01a].

In this study, we employ the FastICA [Hyv01a] on MR perfusion images to develop a systematic method for multi-tissue hemodynamic classification and delineation of an appropriate in-plane AIF. The hemodynamic parameter maps, rCBV, rCBF and rMTT, of each segmented region are subsequently quantified. The use of ICA is motivated by two

inherent assumptions: 1) partial volume mixing, that is, signal intensity of each pixel is a linear mixture contributed from different tissues; and 2) the spatially anatomic structures of pure types do not overlap with each other and their corresponding signal-time curves are distinct from each other. The whole classification process is looped by two alternative steps: 1) the first step is to identify a major tissue type on each independent image resulted from FastICA based on the corresponding signal-time curve, and 2) the second step is to automatically extract regions of the major tissue from a selected independent image by using an optimal thresholding [Ots79a]. All pixels belonging to the tissue of interest are removed from the perfusion images and number of independent components decreases by one before the loop continues. Among all tissues of interest, arterial compartment is first extracted to model an in-plane arterial input function (AIF), which in turn is used to compute the rCBV, rCBF and rMTT maps on a pixel-by-pixel basis. Once all tissues of interest (artery, vein and sinus, choroid plexus, gray matter, white matter, etc.) are dissected, their averaged (true) signal-time curves, concentration time curves, rCVB, rCBF and rMTT maps are computed.

## 2. MATERIAL AND METHOD

### Subjects and Data Recording

Five healthy volunteers aged from 18 to 47 participated in this study. They were 3 males and 2 females with body weights between 49 and 70 kg. Written informed consent was obtained from each volunteer before this study. A multi-slice gradient-echo EPI pulse sequence on a 1.5 Tesla scanner (Signa® CV/i, GE Medical Systems, Milwaukee, WI, USA) was used to acquire the dynamic perfusion images. The imaging parameters were trans-axial imaging, TE/TR = 60/1000 ms, flip angle = 90 degree, FOV = 24 cm × 24 cm, matrix = 128×128, slice thickness/gap = 5/5 mm for 7 slices, one acquisition, and 100 images per slice location. Twenty ml of Gd-DTPA-BMA (Omniscan®, 0.5 mmol/ml, Nycomed Imaging, Oslo, Norway) followed by 20 ml of normal saline were delivered administratively by a power injector (Spectris®, Medrad, Indianola, PA, USA) at a flow rate of 3-4 ml/sec in an antecubital vein. Figure 1 exhibits the 15<sup>th</sup> through 34<sup>th</sup> perfusion images trans-axially through the body of lateral ventricle encompassing the first pass of circulation for a volunteer (a 18 year-old female). The temporal resolution is one second. Since we are only interested in the dynamic images which have stable baselines and discernibly temporal signal changes, the first three and last twenty-seven images were removed from 100 images and seventy ones were kept in a slice location for analysis. All the

routines were implemented using MATLAB (MathWorks, Inc., Natick, MA) code and performed on a 2 G-Hz Pentium-based personal computer.

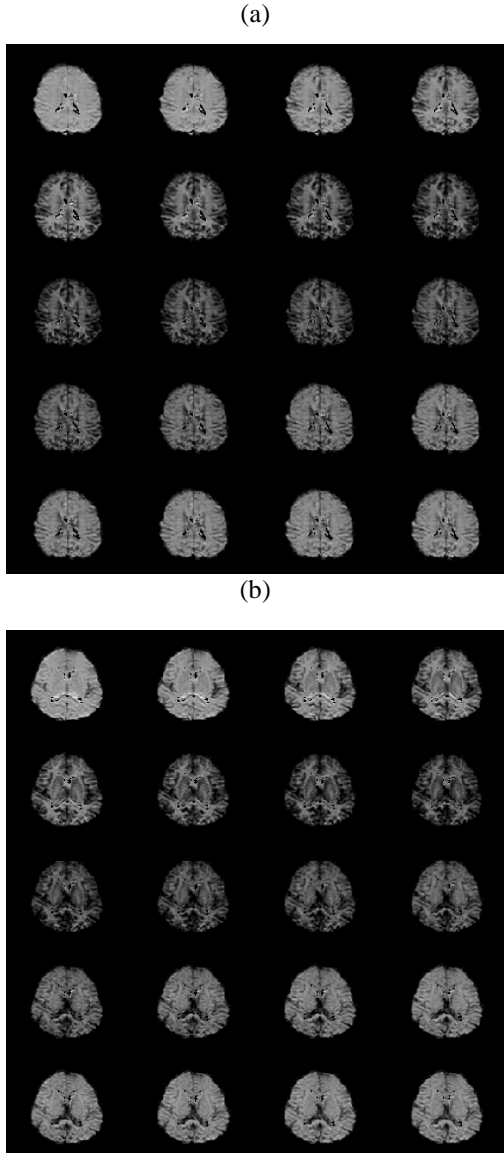


**Figure 1** Dynamic perfusion images (from left to right, top to bottom) at the upper (a) and middle (b) slice locations encompass the first circulation from a 18 year-old volunteer.

### Data Pre-processing

The brain regions were extracted from the perfusion images by first setting all pixel values larger than 15% of the maximum intensity to one and all values smaller than this threshold to zero. An erosion operation with a 3x3 structure element were applied to the resultant binary mask in removing pixels corresponding to skull and scalp areas, followed by a dilation operation with 5x5 structure element in filling holes of the brain region. In addition, spatial or temporal filtering could also be used to increase the

signal-to-noise level. The area of cerebral spinal fluid (CSF) was also removed from the perfusion images before ICA analysis. Since the region of CSF usually contains much fewer pixels compared to those of other tissue types, the statistics resulting from insufficient samples makes the CSF difficult to be distinguished from other tissue types using ICA.

The region of CSF, however, can be identified manually under the assumption that the contrast agent doesn't enter the CSF massively (although little diffusion is possible) so that the pixels values of CSF remain relatively constant. To facilitate the CSF segmentation, we drawn region of interest around the CSF area on the image, which has the maximum intensity decrease compared with the baseline images, and selected the brighter pixels whose signal time curves are relatively constant. Only the pixels within the extracted brain region excluding CSF were subjected to further segmentation process.

### Assumption of linear partial volume mixing on perfusion image

The effect of *partial volume mixing* appears when a pixel represents a combination of materials due to the finite resolution of imaging process. Assume that there are  $q$  pure tissue types presented on perfusion images and that signal intensity of each pixel is a linear combination of contributions from  $q$  pure tissues. If there are  $v$  pixels (without air background and CSF) for each image, the observation of  $p$  temporal images can be denoted by a  $p \times v$  matrix  $\mathbf{X}$ , i.e., each row is an image and each column is the signal intensities of a pixel through  $p$  time points. Based on the premise of partial volume mixing, the observation matrix can be expressed as follows:

$$\mathbf{X} = \mathbf{M} \mathbf{F} \quad (1)$$

$p \times v$        $p \times q$      $q \times v$

where  $\mathbf{M}$  is a  $p \times q$  mixing matrix with each column representing a signal-time curve for a pixel occupied by a pure tissue type, and  $\mathbf{F}$  is a  $q \times v$  partial-volume matrix with each row representing a partial-volume image (value of each element between zero and one) for a tissue type. An intermediate step of proposed method is the use of ICA to recover the partial-volume matrix  $\mathbf{F}$  from the only available signals  $\mathbf{X}$ , and identify the tissue type of each partial-volume image (row vector) in  $\mathbf{F}$ .

### Independent Component Analysis

The ICA methods were developed to separate observed signals into statistically independent source signals [Bel95a, Jun01a, Hyv01a]. To apply ICA to perfusion images, each row of  $\mathbf{X}$  (or  $\mathbf{F}$ ) in Eq. (1) is treated as samples generated from random variables, say  $x_i$  (or  $f_i$ ),  $i = 1, 2, \dots, p$ , or random vector  $\mathbf{x}$  (or  $\mathbf{f}$ ). The partial-volume images in  $\mathbf{F}$ , which exhibit

distinct tissues, are further assumed to be spatially independent: the joint probability distribution for all  $f_i$ 's can be factorized into the product of individual probability distributions, *i.e.*,

$$P(f_1, \dots, f_p) = P(f_1) \cdots P(f_p).$$

The ICA techniques find a  $q \times p$  unmixing matrix,  $\mathbf{W}$ , which converts the random vector  $\mathbf{x}$  into another random vector,  $\mathbf{c} = \mathbf{W}\mathbf{x}$ , that is as mutually independent as possible.

All calculations in the present study were carried out using the FastICA algorithm which features high speed calculation (cubic convergence) and does not require choice of the step size parameters or learning rate as compared to the gradient-based algorithm [Hyv97a, Hyv01a]. The FastICA technique first removes means of row vectors in the  $\mathbf{X}$  sample matrix followed by a whitening process implemented by the principal component analysis (PCA). Each random variable  $x_i$  becomes zero-mean and the covariance matrix of the whitened data becomes an identity matrix. The whitening process provides an advantage that the sources or independent components may be estimated from the first  $N$  ( $N \leq p$ ) largest principal components, which interpret the greatest amount of variance. After whitening, only the first  $N$  most significant principal components are preserved in the subsequent FastICA calculation. The next step is to look for a matrix that transforms the whitened data into a set of components as mutually independent as possible. Mutual information, as a measure of the independence of random variables, is used as the criterion for finding such a transformation. Hyvarinen has shown that mutual information can be expressed in terms of negentropy for measuring non-Gaussianity [Hyv97a, Hyv01a]. Therefore, the problem of finding the independent components ( $\mathbf{c}$ ) and the transform matrix ( $\mathbf{W}$ ) can be translated into a search for linear combinations of the whitened data that maximize the negentropy of the distributions of  $c_i$ , for  $i = 1, \dots, N$ . The FastICA estimates such an optimal transformation  $\mathbf{W}$  and produces the independent components in a matrix form:  $\mathbf{C} = \mathbf{W}\mathbf{X}$ . Each row in  $\mathbf{C}$  is referred to as the independent component (IC) image and is related to one of the partial-volume images described by the rows of  $\mathbf{F}$  matrix. Ideally,  $\mathbf{C}$  and  $\mathbf{F}$  are the same except that their rows differ from permutation and scaling (including the signs reverse). The signal-time curves for the independent-component images can be obtained from the columns of pseudo-inverse of matrix  $\mathbf{W}$ .

### Sequential FastICA Processing And Automatic Thresholding

Before the FastICA was carried out, we needed to determine the number of IC images ( $N$ ), that is,

number of tissue type ( $q$ ,  $q=N$  in this study). This can be done by either evaluating the eigenvalues which have dominant variances of the perfusion images, or computing Akaike information index [Aka74a], which employed information theoretic method to determine the model complexity. Our results, nevertheless, indicated that neither method provided the index curves with sharp drop at certain number and ended up with indecisive solution. To decide the number of IC images, we have experimented with various  $N$  values, ranging from 3 up to 7, and inspected the outcomes. The IC images at  $N = 5$  exhibited distinctly discernible tissue types and appeared to agree with our knowledge of brain anatomy and physiology, that is artery, VS, GM, WM and CP.

We have experienced that if the FastICA was applied only once, the output independent component (IC) images provided coarse segmentations and usually consisted of two or three tissue types of which one was dominant. The contribution from minor tissue types within the same IC image may contaminate the signal-time curve of the major tissue type. Besides, the corresponding signal-time curve of each IC image was rescaled during the FastICA optimization process, which cannot be used for the calculation of hemodynamic parameters. To obtain accurate classification and true signal-time curve of each tissue type, the whole process was looped by repeatedly using FastICA following by a thresholding. In each loop, only one IC image was selected and brighter pixels were segmented out by an automatic threshold to represent a dominant tissue type. The selection order of IC images was determined based on a priori knowledge of the spatial and temporal characteristics of each tissue type. In general, the contrast agent arrives first at the artery, followed by gray matter, white matter, VS or CP (while, CP contains mixtures of arteriole, capillary and venule and present a group of multi-phasic hemodynamics). The selection of IC images started with the one containing artery as the major tissue type since the corresponding signal time curve has the fastest signal drop and can be easily identified. Next, we selected the IC images whose dominant tissues consisting of fewer pixels. This is because the fewer pixels are within a cluster, the shaper is their distribution and the more reliable is the computed threshold and segmentation results. Usually VS or CP consists of fewer pixels than that of gray matter and white matter. Taking both the spatial and temporal considerations into account, the rules of thumb for the selection order were: 1) in the first loop, select the IC image where the major tissue type was artery; 2) in the next two loops, select the IC images where the major tissue types have fewer pixels, e.g. VS or CP; and 3)

in the last loop, select the IC image whose major type was gray matter. Once a tissue type was identified at each loop, the intensities of associated pixels were averaged to produce the true signal-time curve and these pixels were deleted from the perfusion data before next loop. The number of IC images was reduced by one after each loop. The loop continues until all the pixels were classified. The last IC image was considered as white matter due to its flattest distribution.

The Otsu's method [Ots79a] was utilized to automatically determine a threshold in segmenting gray-scaled IC images. The procedure of this method is unsupervised and computationally effective since only the zeroth- and first-order cumulative moments of the gray-level histogram were calculated. In our applications, the larger value from two thresholds for the three-class separation were determined for most tissue types, and one threshold for the two-class separation was determined for gray matter due to its dispersive distribution. In addition, manual adjustment of the threshold was provided as an additional option for IC images, which was used only when their histograms were fairly flat.

### Calculation of parametric images for relative CBV (rCBV), relative CBF (rCBF) and relative MTT (rMTT)

Pixel-by-pixel parametric maps for CBV, CBF, and MTT were calculated for areas of classified tissues using the concentration-time curves. The concentration time curve  $c_i(t)$  for a pixel was computed by the linear relationship with the change of relaxation rate,  $\Delta R_2^*(t)$ :

$$c_i(t) = \Delta R_2^*(t) = -\frac{k}{TE} \ln\left(\frac{S(t)}{S_0}\right) \quad (2)$$

where  $k$  is an unknown constant,  $TE$  was the echo time, and  $S(t)$  and  $S_0$  were the signal intensities of each pixel at time  $t$  and at the baseline, respectively [Ost96a, Rem94a, Ros90a, Fis91a, Wei94a]. Note that the concentration-time curve for the artery region on the same slice was used as an AIF, i.e.,  $c_a(t)$ , in the following computation of rCBV and rCBF. By using the indicator dilution theory, one can determine the rCBV as a ratio of the area integrating over the first pass of a contrast agent under the concentration-time curve,  $c_i(t)$ , to that under the AIF [Mei54a, Zie62a]:

$$rCBV = \frac{\int_{\text{first pass}} c_i(t) dt}{\int_{\text{first pass}} c_a(t) dt} \quad (3)$$

The rCBF can be computed based on the relationship with concentration-time curve for a pixel of tissue:

$$c_i(t) = rCBF \cdot c_a(t) \otimes R(t) \quad (4)$$

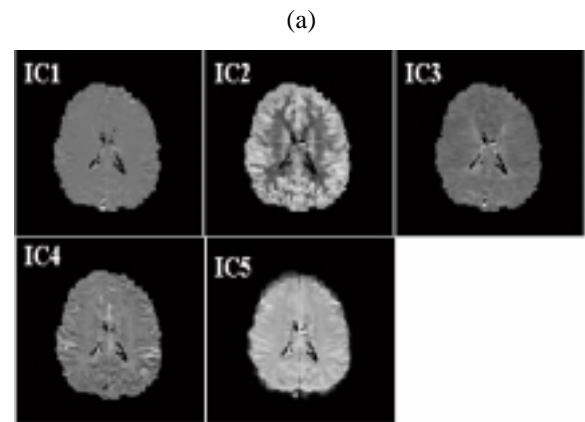
where  $\otimes$  denotes convolution,  $\cdot$  denotes multiplication and  $R(t)$  is the residue function for the pixel [Ket60a]. The singular value decomposition (SVD) method [Ost96a] was employed and implemented to deconvolve Eq. (4) and calculate the  $rCBF \cdot R(t)$  curve for each pixel. To minimize the oscillation effect on the solution, small singular values in the diagonal matrix produced by SVD were set to be zeros. The cut-off threshold was chosen as 20% of the maximum singular value [Ost96a]. The value of rCBF, in theory, can be determined by the initial value of deconvolved curve, i.e.  $R(t=0) = 1$ , according to the indicator dilution theory. However, the AIF can be affected by a time delay and dispersion of the bolus, causing the spreading of deconvolved curve. Ostergaard et al. suggested that the maximum value of  $rCBF \cdot R(t)$  curve should be used instead of value at initial point to avoid underestimate of the flow.

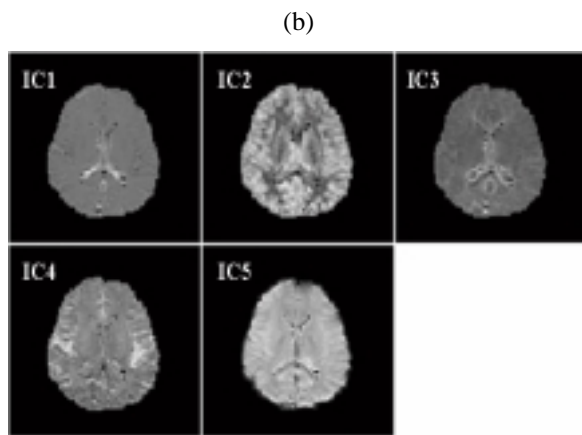
The rMTT of contrast-agent particles passing through a pixel can be calculated using the central volume principle [Rem94a, Ros90a; Ost96a]:

$$rMTT = \frac{rCBV}{rCBF} \quad (5)$$

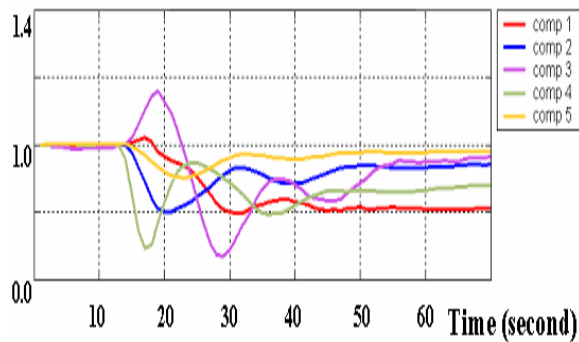
### 3. RESULTS

Figures 2 and 3 show the resultant five IC images and the corresponding signal-time curves from the first loop of ICA computation with  $N$  (the number of independent components) = 5, respectively. The signal time curves were all normalized to unit variance and their baselines were shifted to 1.0 for the comparison. The arterial component (component 4) in Fig. 3 can be easily identified due to the fastest signal drop.





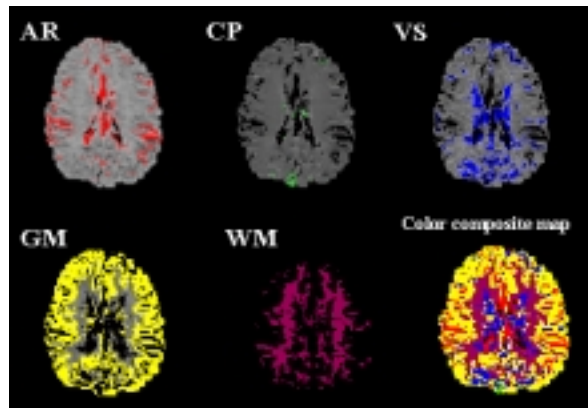
**Figure. 2** Five IC images of the upper slice location (a) and the middle slice location (b) produced from the first loop.



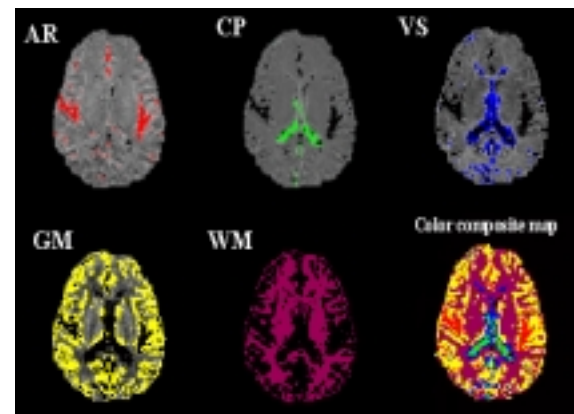
**Figure. 3** The normalized signal-time curves corresponding to five IC images. The Component 4 can be easily identified as artery signal because of its fastest signal drop.

Figure 4 and 5 depict the final results with five segmented tissue types, *i.e.*, artery, CP, VS, GM, WM and their color-coded composite images. In order to analyze the hemodynamics, different colored areas of composite images at both upper and middle slice locations were used as region of interests to compute the average signal-time curves of different tissue types (see Fig. 6).

Figure 7 (a) and (b) show the normalized concentration-time curves of five tissue types at the upper and middle slice locations, respectively. The concentration-time curves for the artery regions (red ones) at these two slice locations were modeled respectively as arterial input functions for subsequent relative CBF deconvolution calculations. Figure 8 (a) and (b) present parametric images for relative CBV (left), relative CBF (middle), and relative MTT (right) at the upper and middle slice locations, respectively.



**Figure 4.** The final segmentation result for each tissue type at the upper slice location and their color composite map. .



**Figure. 5** The final segmentation result for each tissue type at the middle slice location and their color composite map. .

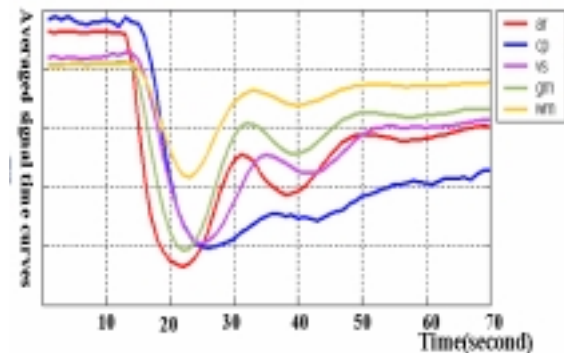


**Figure. 6** The averaged signal-time curves of corresponding segmented tissues at both upper and middle slice locations.

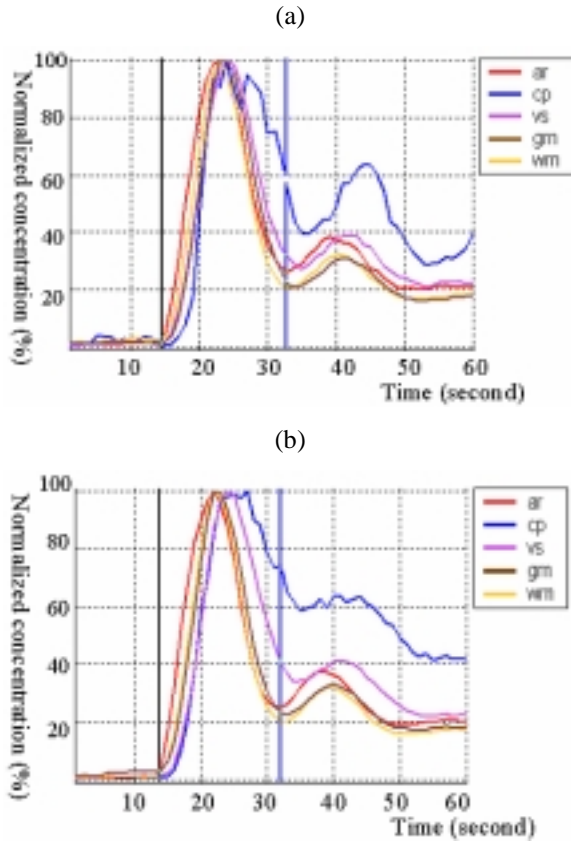


**Figure 7.** The concentration-time curves of five tissue types, artery, CP, GM, WM, VS, at the upper slice location (a) and at the middle slice location (b). The two vertical lines (blue and black lines) indicate the start and end of first pass of artery (red curve).

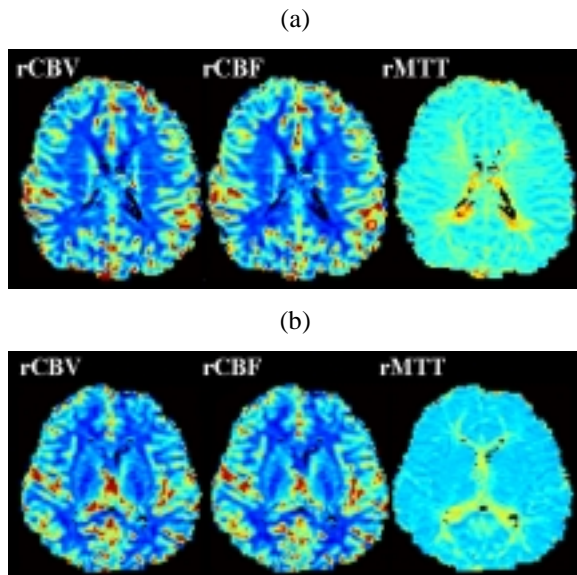


**Figure 8** The parametric images for relative CBV (left), relative CBF (middle), and relative MTT (right) at the upper slice location (a) and at the middle slice location (b). The red and deep blue colors represent the maximum and minimum values, respectively.

Segmentation results of the five subjects (two slice locations for each subject) of perfusion images can be summarized as follows: 1) artery areas were reliably segmented using  $N=5$ ; 2) the contrast agent was consistently observed to arrive first at the artery, followed by GM, WM, VS and CP; and 3) the averaged ratios (shown in Table 1) for relative CBV, relative CBF, and relative MTT between gray matter and white matter were in good agreement with those in the literature [Cal99a].

	Upper slices (mean $\pm$ std)	Middle slices (mean $\pm$ std)
rCBV	2.2882 $\pm$ 0.2774	2.1256 $\pm$ 0.5178
rCBF	2.3376 $\pm$ 0.2199	2.2238 $\pm$ 0.5568
rMTT	0.9964 $\pm$ 0.0544	0.9542 $\pm$ 0.0661

**Table 1** The averaged ratios for hemodynamic parameters between gray matter and white matter.

#### 4. CONCLUSIONS

In conclusion, the proposed method for analyzing perfusion images has several advantages: 1) the systematic classification of tissues with different hemodynamic patterns; 2) the delineation of sequential passage of contrast agent to these tissues; and 3) the effective modeling of an arterial input function on the same slice location for the calculations of relative CBV, relative CBF and relative MTT. The resultant information on hemodynamics will further expand our knowledge of cerebral blood circulation in human brains

#### 5. ACKNOWLEDGMENTS

The study was funded by the Ministry of Education of Taiwan (89BFA221401), the Taipei Veterans General Hospital, Taiwan (91380), and the National Science of Council, Taiwan (NSC-922218E010016).

#### 6. REFERENCES

- [Aka74a] Akaike, H. A new look at statistical model identification. *IEEE Transactions on Automatic Control* **19**:716-723,1974.
- [Arf02a] Arfanakis, K., Cordes, D., Haughton, V. M., Carew, J. D. and Meyerand, M. E. Independent component analysis applied to diffusion tensor MRI. *Magnetic Resonance in Medicine* **47**:354-363, 2002.
- [Aro95a] Aronen, H. J., Glass, J., Pardo, F. S., Belliveau, J. W., Gruber, M. L., Buchbinder, B. R., Gazit, I. E., Linggood, R. M., Fischman, A. J., Rosen, B. R. and Hochberg, F. H. Echo-planar MR cerebral blood volume mapping of gliomas. *Acta Radiologica* **36**:520-528, 1995.
- [Bel95a] Bell, A. J. and Sejnowski, T. J. An information-maximization approach to blind separation and blind deconvolution. *Neural Computation* **7**:1129-1159, 1995.

- [Cal99a] Calamante, F., Thomas, D. L., Pell, G. S., Wiersma, J. and Turner, R. Measuring cerebral blood flow using magnetic resonance imaging techniques. *Journal of Cerebral Blood Flow and Metabolism* **19(7)**:701-735, 1999.
- [Car02a] Carroll, T. J., Haughton, V. M., Rowley, H. A. and Cordes, D. Confounding effect of large vessels on MR perfusion images analyzed with independent component analysis. *American Journal of Neuroradiology* **23**:1007-1012, 2002.
- [Fis91a] Fisel, C. R., Ackerman, J. L., Buxton, R. B., Garrido, L., Belliveau, J. W., Rosen, B. R. and Brady, T. J. MR contrast due to microscopically heterogeneous magnetic susceptibility: numerical simulation and applications to cerebral physiology. *Magnetic Resonance in Medicine* **17**:336-347, 1991
- [Guc96a] Guckel, F. J., Brix, G., Schmiedek, P., Piepgras, Z., Becker, G., Kopke, J., Gross, H. and Georgi, M. Cerebrovascular reserve capacity in patients with occlusive cerebrovascular disease: assessment with dynamic susceptibility contrast-enhanced MR imaging and the acetazolamide stimulation test. *Radiology* **201(2)**:405-12, 1996.
- [Hyv97a] Hyvarinen, A. and Oja, E. A fast fixed-point algorithm for independent component analysis. *Neural Computation* **9(7)**:1483-1492, 1997.
- [Hyv01a] Hyvarinen, A., Karhunen, J. and Oja, E. Independent component analysis, *John Wiley & Sons, Inc., New York*. 2001.
- [Jun01a] Jung, T. P., Makeig, S., Westerfield, M., Townsend, J., Courchesne, E. and Sejnowski, J. T. Analysis and visualization of single-trial event-related potentials. *Human Brain Mapping* **14**:166-185, 2001.
- [Ket60a] Kety, S. S. Blood-tissue exchange methods: Theory of blood-tissue exchange and its application to measurement of blood flow. *Methods Med. Res.* **8**:223-227, 1960.
- [Lee01a] Lee, J. S., Lee, D. S., Ahn, J. Y., Cheon, G. J., Kim, S. K., Yeo, J. S., Park, K. S., Chung, J. K., Lee, M. C. Blind separation of cardiac components and extraction of input function from H<sub>2</sub><sup>15</sup>O dynamic myocardial PET using independent component analysis. *J. Nucl. Med.* **42(6)**:938-943, 2001.
- [Lee03a] Lee, P. L., Wu, Y. T., Chen, L. F., Chen, Y. S., Cheng, C.M., Yeh, T. C., Ho, L. T., Chang, M. S., and Hsieh, J. C. ICA-based spatiotemporal approach for single-trial analysis of post-movement MEG beta synchronization. *NeuroImage* in press, 2003.
- [Mei54a] Meier, P. and Zierler, K. L. On the theory of the indicator-dilution method for measurement of blood flow and volume. *Journal of applied physiology* **6**:731-744, 1954.
- [Ost96a] Ostergaard, L., Sorensen, A. G., Kwong, K. K., Weisskoff, R. M., Gyldensted, C. and Rosen, B. R. High resolution measurement of cerebral blood flow using intravascular tracer bolus passages. Part II: Experimental comparison and preliminary results. *Magnetic Resonance in Medicine* **36(5)**:726-736, 1996.
- [Ots79a] Otsu, N. A threshold selection method from gray-level histograms. *IEEE Transactions on System, Man, And Cybernetics* **SMC-9(1)**:62-66, 1979.
- [Rem94a] Rempp, K. A., Brix, G., Wenz, F., Becker, C. R., Guckel, F. and Lorenz, W. J. Quantification of regional cerebral blood flow and volume with dynamic susceptibility contrast-enhanced MR imaging. *Radiology* **193(3)**:637-41, 1994.
- [Rog94a] Rogowska, J., Preston, K., Aronen, H. J. and Wolf, G. L. A comparative analysis of similarity mapping and eigenimaging as applied to dynamic MR imaging of a low grade astrocytoma. *Acta Radiologica* **35(4)**:371-377, 1994.
- [Ros90a] Rosen, B. R., Belliveau, J. W., Vevea, J. M. and Brady, T. J. Perfusion imaging with NMR contrast agents. *Magnetic Resonance in Medicine* **14**:249-265, 1990.
- [Sor97a] Sorensen, A. G., Tievsky, A. L., Ostergaard, L., Weisskoff, R. M. and Rosen, B. R. Contrast agents in functional MR imaging. *Journal of Magnetic Resonance Imaging* **7(1)**:47-55, 1997.
- [Wei94a] Weisskoff, R. M., Zuo, C. S., Boxerman, J. L. and Rosen, B. R. Microscopic susceptibility variation and transverse relaxation: theory and experiment. *Magnetic Resonance in Medicine* **31(6)**:601-610, 1994.
- [Wia01a] Wiart, M., Rognin, N., Berthezene, Y., Nighoghossian, N., Froment, J. C. and Baskurt, A. Perfusion-based segmentation of the human brain using similarity mapping. *Magnetic Resonance in Medicine* **45(2)**:261-268, 2001.
- [Zie62a] Zierler, K. L. Theoretical basis of indicator-dilution methods for measuring flow and volume. *Circulation Research* **10**:393-407, 1962.
- [Zie65a] Zierler, K. L. Equations for measuring blood flow by external monitoring of radioisotopes. *Circulation Research* **16**:309-321, 1965.